GENE REGULATION

SLAM-seq defines direct gene-regulatory functions of the BRD4-MYC axis

Matthias Muhar,[1] Anja Ebert,[1] Tobias Neumann,[1] Christian Umkehrer,[1] Julian Jude,[1] Corinna Wieshofer,[2] Philipp Rescheneder,[3] Jesse J. Lipp,[1] Veronika A. Herzog,[4] Brian Reichholf,[4] David A. Cisneros,[1] Thomas Hoffmann,[1] Moritz F. Schlapansky,[1] Pooja Bhat,[4] Arndt von Haeseler,[3] Thomas Köcher,[5] Anna C. Obenauf,[1] Johannes Popow,[2] Stefan L. Ameres,[4]* Johannes Zuber[1,6]*

Defining direct targets of transcription factors and regulatory pathways is key to understanding their roles in physiology and disease. We combined SLAM-seq [thiol(SH)–linked alkylation for the metabolic sequencing of RNA], a method for direct quantification of newly synthesized messenger RNAs (mRNAs), with pharmacological and chemical-genetic perturbation in order to define regulatory functions of two transcriptional hubs in cancer, BRD4 and MYC, and to interrogate direct responses to BET bromodomain inhibitors (BETis). We found that BRD4 acts as general coactivator of RNA polymerase II–dependent transcription, which is broadly repressed upon high-dose BETi treatment. At doses triggering selective effects in leukemia, BETis deregulate a small set of hypersensitive targets including MYC. In contrast to BRD4, MYC primarily acts as a selective transcriptional activator controlling metabolic processes such as ribosome biogenesis and de novo purine synthesis. Our study establishes a simple and scalable strategy to identify direct transcriptional targets of any gene or pathway.

Transcription factors (TFs) and chromatin regulators govern the identity and fate of a cell, and their mutation or dysregulation drives cancer and other human diseases (*1*). Epigenetic regulators that maintain aberrant cell states have emerged as accessible entry points for targeted therapies (*2*). Among these, BET bromodomain inhibitors (BETis) have shown activity in preclinical models of leukemia and other cancers (*2*, *3*), yet underlying mechanisms remain poorly understood. Although BETis interfere with multiple BET proteins, therapeutic effects have mainly been attributed to displacement of BRD4 from acetylated histones and repression of its target genes. In hematopoietic malignancies, BETis commonly trigger repression of *MYC* (*4*–*6*), an oncogenic TF that is overexpressed in up to 70% of human cancers (*7*).

Defining direct targets of transcriptional regulators such as BRD4 and MYC is critical, both for understanding their cellular function and for therapy development. However, deciphering direct regulatory relationships remains challenging because genomic binding of a factor does not predict regulatory functions on neighboring genes, whereas conventional expression analyses after gene perturbation preclude a clear distinction between direct and indirect effects owing to vast differences in mRNA and protein half-lives (fig. S1A) (*8*, *9*). An ideal strategy for defining direct transcriptional targets would combine rapid protein perturbation and subsequent measurement of changes in mRNA output at time scales that preclude secondary effects.

Thiol(SH)–linked alkylation for the metabolic sequencing of RNA (SLAM-seq) enables the direct quantification of 4-thiouridine (4sU)–labeled mRNAs within the total mRNA pool (*10*). This is achieved through alkylation of the thiol group in 4sU (fig. S1B), which prompts misincorporation of G during reverse transcription, enabling the detection of 4sU as thymine-to-cytosine (T>C) conversion in 3′-end mRNA-sequencing. To test the suitability of SLAM-seq for detecting immediate and global changes in mRNA production, we measured responses to inhibition of CDK9, a cyclin-dependent kinase globally required for releasing RNA polymerase II (Pol2) from promoter-proximal pausing (*11*). To this end, we treated human K562 leukemia cells with the CDK inhibitor flavopiridol and performed SLAM-seq after 45 min of 4sU labeling (fig. S1C). As expected, only a few transcripts showed deregulation at the total mRNA level, whereas transcripts containing T>C conversions were broadly repressed (fig. S1, D and E). We further optimized the setup to eliminate noise introduced by polymerase chain reaction and sequencing errors (fig. S1F) and to maximize the recovery of labeled reads (fig. S1G). To test whether SLAM-seq captures more specific transcriptional responses, we treated K562 cells with small-molecule inhibitors of their driving oncogene BCR-ABL, as well as the kinases Mek and Akt, which act in distinct signaling cascades downstream of BCR-ABL (fig. S2A) (*12*). SLAM-seq revealed prominent immediate responses to these inhibitors (fig. S2, B and C) that were not biased by mRNA half-lives (fig. S2D). Combined inhibition of Mek and Akt approximated to effects of BCR-ABL inhibition, recapitulating their function as key effector pathways of BCR-ABL (fig. S2, E and F). Together, these pilot studies establish SLAM-seq as a rapid and scalable approach for probing direct transcriptional responses to drug treatment.

To generalize this approach for investigating the vast number of regulators for which, as in the case of BRD4, no selective inhibitors are available, we sought to combine SLAM-seq with chemical-genetic protein degradation (Fig. 1A). To achieve sufficiently rapid kinetics, we used the auxin-inducible degron (AID) system reported to degrade AID-tagged proteins within less than 1 hour (*13*). Specifically, we introduced a minimal AID-tag into the BRD4 locus of K562 cells (Fig. 1B) and transduced homozygous knock-in clones with a lentiviral vector expressing the rice F-box protein transport inhibitor response 1 (Tir1), which mediates ubiquitination of AID-tagged proteins upon treatment with IAA (indole-3-acetic acid). IAA treatment of edited cells triggered a highly specific and near-complete degradation of BRD4 within 30 min (Fig. 1B; fig. S3, A to C; and table S1). Whereas introduction of the tag or Tir1 expression and IAA treatment were well tolerated, prolonged BRD4 degradation strongly suppressed cell proliferation (fig. S3, D and E) in line with its essential function (*14*).

SLAM-seq after acute BRD4 degradation and 60 min of 4sU labeling revealed a global downregulation of transcription (Fig. 1C and fig. S3F), similar to effects of CDK9 inhibition. These effects are not due to displacement of core transcriptional machinery because loss of BRD4 did not impair chromatin binding of factors involved in transcriptional initiation (TBP1 and MED1) or pause-release and elongation (CDK9, Cyclin T1, and SPT5) (Fig. 1D). Whereas initiation-associated phosphorylation of Pol2 at serine 5 (S5) of its C-terminal repeat domain was unaffected, BRD4 degradation led to a marked reduction of elongation-associated serine 2 (S2)–phosphorylated Pol2, indicating a defect in promoter proximal pause release. Spike-in controlled chromatin immunoprecipitation (ChIP)–sequencing upon BRD4 degradation showed an accumulation of total and S5-phosphorylated Pol2 levels at active transcription start sites (TSSs), whereas total, S5-, and S2-phophorylated Pol2 were reduced throughout gene bodies (Fig. 1, E and F, and fig. S4). These results are in line with a recent report showing a widespread reduction of transcription upon pan-BET protein degradation independent of CDK9 recruitment (*15*) and convincingly show that BRD4 globally controls transcription by promoting the release of stalled Pol2.

Although these findings are consistent with the promiscuous binding of BRD4 to active TSS

[1]Research Institute of Molecular Pathology (IMP), Vienna BioCenter (VBC), 1030 Vienna, Austria. [2]Boehringer Ingelheim–Regional Center Vienna GmbH and Company KG, 1121 Vienna, Austria. [3]Center for Integrative Bioinformatics Vienna, Max F. Perutz Laboratories, University of Vienna and Medical University of Vienna, 1030 Vienna, Austria. [4]Institute of Molecular Biotechnology of the Austrian Academy of Sciences (IMBA), VBC, 1030 Vienna, Austria. [5]Vienna Biocenter Core Facilities (VBCF), 1030 Vienna, Austria. [6]Medical University of Vienna, VBC, 1030 Vienna, Austria.
***Corresponding author. Email: johannes.zuber@imp.ac.at (J.Z.); stefan.ameres@imba.oeaw.ac.at (S.L.A.)**

(*16*), they contrast with selective effects of BETis, which have been widely reported based on results of conventional expression analyses. To define immediate transcriptional responses to BETis, we performed SLAM-seq after treatment with different doses of the BETi JQ1 (*17*) in K562 and human MV4-11 acute myeloid leukemia (AML) cells. In both cell types, high-dose JQ1 treatment (1 or 5 μM) broadly suppressed transcription (Fig. 2A and fig. S5A) and globally reduced Pol2-S2 phosphorylation (fig. S5B) similar to effects observed after BRD4 degradation, showing that global transcriptional functions of BRD4 are BET bromodomain–dependent. Effects of high-dose BETis on Pol2-S2 phosphorylation were recapitulated after knockdown of BRD4 but not BRD2 or BRD3 (fig. S5, C and D), indicating that global effects of BETis are primarily mediated by BRD4 inhibition and cannot be compensated by other BET proteins.

Because JQ1 doses above 1 μM vastly exceed growth-inhibitory concentrations in AML and other sensitive cell lines, we explored direct transcriptional responses to a more selective dose of 200 nM, which triggers strong antileukemic effects in a wide range of AML models (*4*). In K562 cells, one of few BETi-insensitive leukemia cell lines, 200 nM JQ1 induced a selective deregulation of a small number of transcripts (Fig. 2B). Treatment of two highly sensitive AML cell lines with the same dose triggered transcriptional responses that were comparable in scale (Fig. 2B and fig. S6, A and B) and affected a similar set of BETi-hypersensitive transcripts, including *MYC* and other genes known to be essential in myeloid leukemia cells (Fig. 2C and fig. S6, C and D)

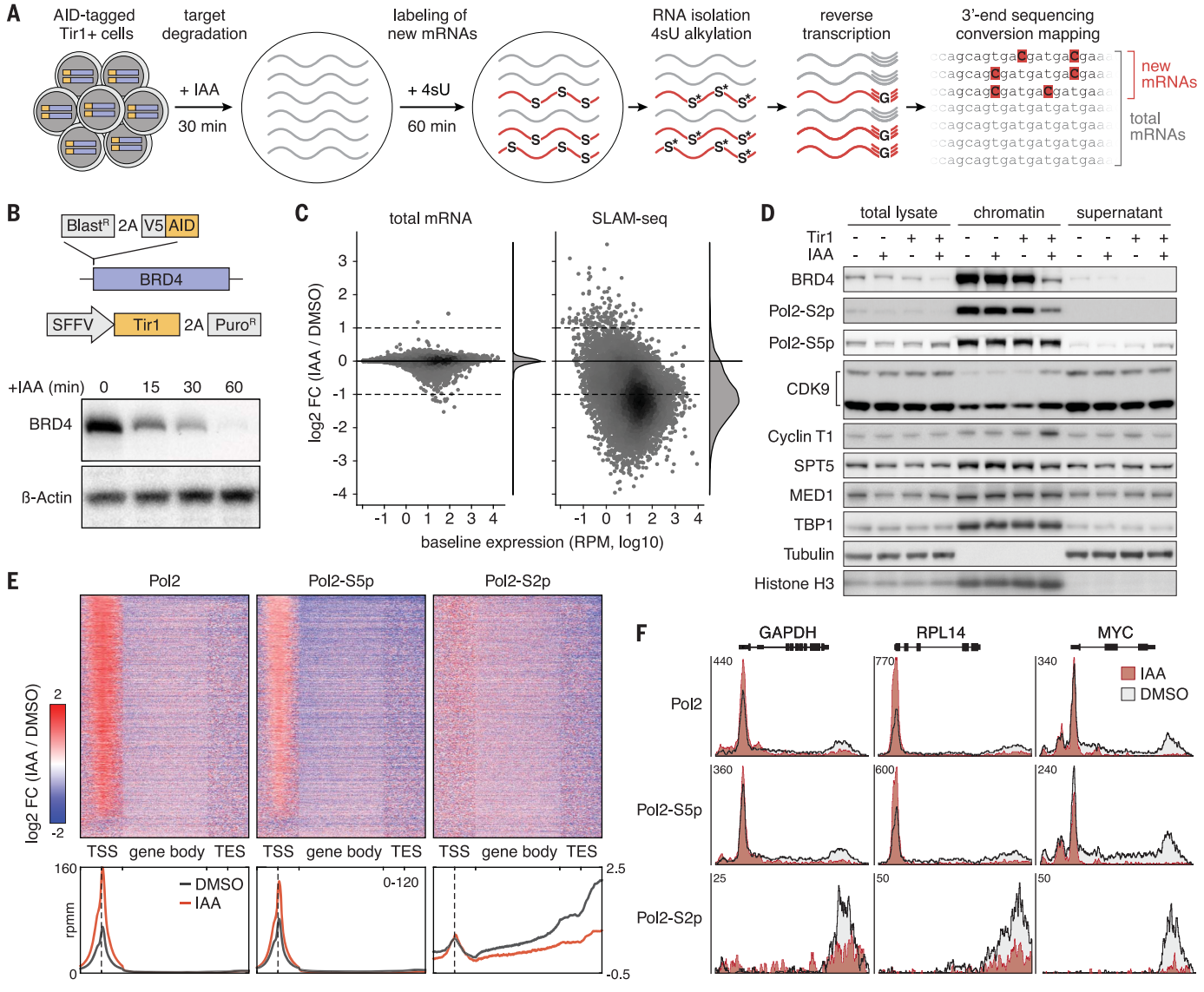

Fig. 1. Global transcriptional control by BRD4. (**A**) Sample workflow of a SLAM-seq experiment mapping direct transcriptional responses to degradation of AID-tagged proteins. (**B**) Schematic of the AID-BRD4 knock-in allele and Tir1 delivery vector SOP (pRRL-SFFV-Tir1-3xMYC-tag-T2A-Puro). Immunoblotting of BRD4 in K562$^{AID\text{-}BRD4}$+Tir1 cells treated with 100 μM IAA for the indicated time points. (**C**) Changes in the abundance of total and newly synthesized mRNAs (detected in SLAM-seq based on T>C conversions) in K562$^{AID\text{-}BRD4}$+Tir1 cells treated with IAA for 30 min followed by 4sU labeling over 60 min. FC, fold-change. (**D**) Immunoblotting of indicated transcriptional core regulators and controls in total cell lysate, chromatin fraction, and supernatant of K562$^{AID\text{-}BRD4}$+Tir1 cells treated with IAA for 60 min. (**E**) Spike-in controlled ChIP-seq of hypophosphorylated, S2-phosphorylated, and S5-phosphorylated Pol2 in K562$^{AID\text{-}BRD4}$+Tir1 cells treated with IAA for 60 min. Heatmaps and density diagrams show change of signals across genes at transcription start sites (TSS, ± 1 kb), gene bodies (scaled), and transcription end sites (TES, ± 1 kb). A density scale from low (blue) to high (red) is shown. rpmm, reads per million mapped reads. (**F**) Changes of Pol2 occupancy upon BRD4 degradation shown in (E) for indicated genes.

(*14*). These findings are in line with the notion that sensitivity to BETis at the cellular level is determined by secondary adaptation rather than differences in the primary transcriptional response (*18*, *19*). We also noted a small set of genes that were commonly up-regulated after BET inhibition or BRD4 degradation (fig. S6E) through mechanisms that remain elusive. Collectively, our results reveal a profound dose-dependency of direct responses to BETis and show that therapeutically active doses trigger antileukemic effects by deregulating a small set of hypersensitive genes.

We next explored whether the BETi hypersensitivity of certain transcripts simply reflects a pronounced sensitivity to interference with general Pol2 pause-release machinery. To test this, we used SLAM-seq to compare transcriptional responses to BET inhibition (200 nM JQ1) to effects triggered by different doses of the selective CDK9 inhibitor NVP-2 (*20*). Whereas high-dose CDK9 inhibition (60 nM NVP-2) globally suppressed transcription, an intermediate dose (6 nM NVP-2) triggered selective transcriptional responses that were distinct from the conserved response to BETis (Fig. 2, D and E, and fig. S7, A and B). Because CDK9 and BET inhibitors display strong synergistic effects (fig. S7, C and D) (*20*), we sought to investigate transcriptional responses underlying this phenomenon. In contrast to selective effects seen after single-agent treatment, combining intermediate doses of JQ1 and NVP-2 triggered a global loss of transcription similar to high-dose CDK9 inhibition (Fig. 2, D and E, and fig. S7A). These observations hold true in a genetically distinct AML cell line (fig. S7, E and F), suggesting that the therapeutic synergy between BETis and CDK9i is largely based on synergistic suppression of global transcription, raising concerns about toxicities of this combination. These results also suggest that therapeutically active doses of CDK9 and BET inhibitors exploit different bottlenecks in Pol2 pause-release to trigger selective transcriptional responses.

To investigate whether BETi hypersensitivity is determined by specific chromatin features at

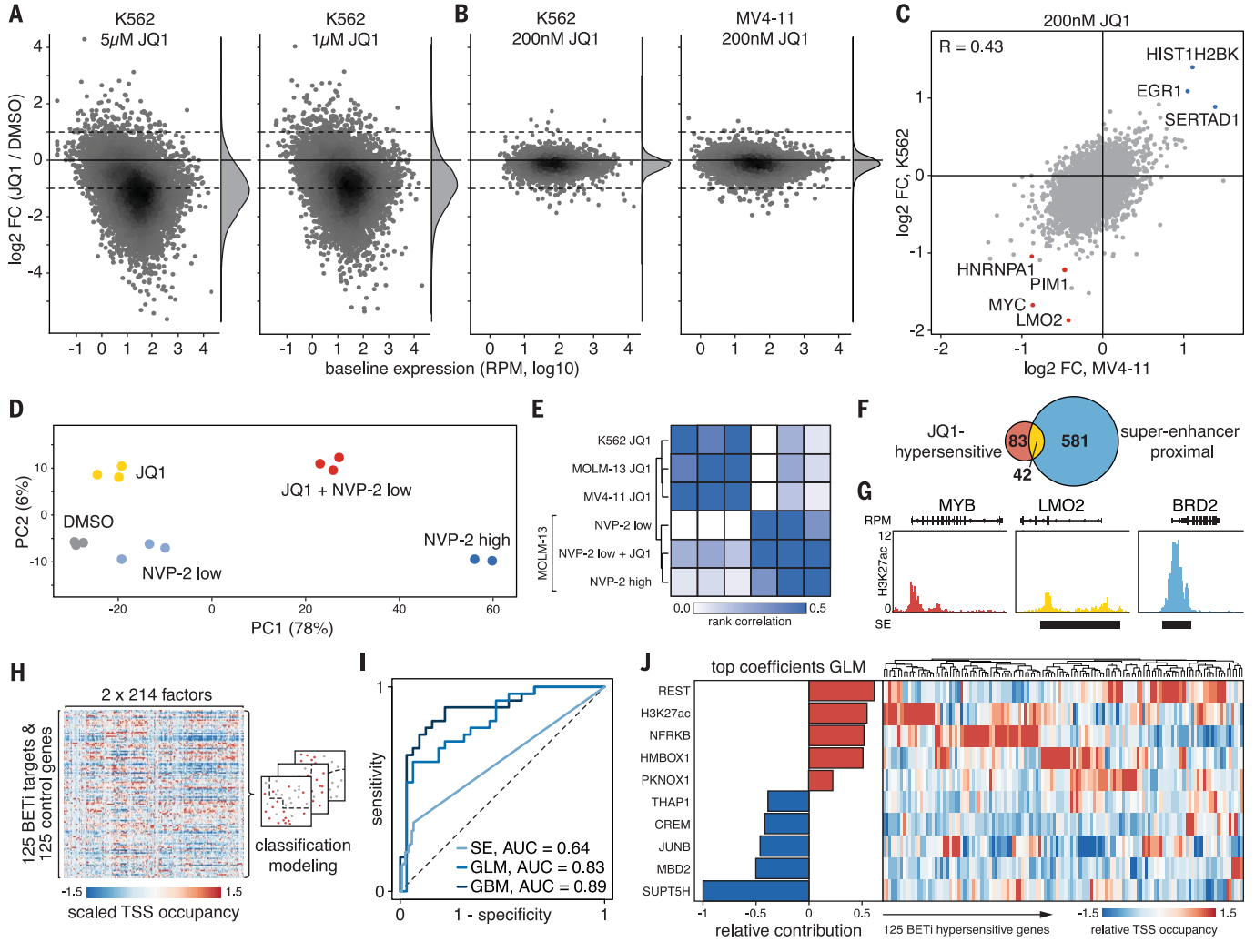

Fig. 2. Dose dependency and determinants of responses to BETis. (**A**) SLAM-seq responses of K562 cells treated with indicated doses of JQ1 for 30 min before 4sU labeling for 60 min. (**B**) SLAM-seq responses of K562 and MV4-11 cells treated with 200 nM JQ1 as in (A). (**C**) Pairwise comparison of SLAM-seq responses to JQ1 shown in (B). *R*, Pearson correlation coefficient. (**D**) Principal component analysis of SLAM-seq profiles from MOLM-13 cells treated with JQ1 or NVP-2 as in (A). (**E**) Heatmap and hierarchical clustering of Spearman's rank correlations between SLAM-seq responses to JQ1 and NVP-2 in indicated cell lines. (**F**) Venn diagram showing overlap between BETi-hypersensitive genes and published superenhancer targets in K562 cells. (**G**) Sample tracks of H3K27ac ChIP-seq with superenhancer (SE) annotation exemplifying categories in (F). (**H**) Simplified model generation workflow for classifying BETi-hypersensitive genes based on 214 chromatin signatures. (**I**) ROC curve for classification of BETi-hypersensitive genes by means of superenhancer assignment or two independent chromatin signature–based models assessed on a held-out test set. (**J**) Relative contribution of the strongest positive and negative predictors to the GLM shown in (I) based on normalized model coefficients. Heatmap shows relative ChIP-seq densities of these factors at TSS of 125 BETi-hypersensitive genes.

target genes, we first tested whether BRD4 occupancy levels at TSS or their accessibility to BETis could distinguish direct BETi targets [false discovery rate (FDR) ≤ 0.1, $\log_2$–fold-change (FC) ≤ −0.7] from an equally sized cohort of unresponsive genes with identical baseline expression (FDR ≤ 0.1, −0.1 ≤ $\log_2$FC ≤ 0.1) (fig. S8A). Whereas chromatin occupancy of BRD4 did not predict BETi-hypersensitive target genes [area under the receiver operating characteristic (ROC) curve (AUC) 0.52] (fig. S8B), recently reported chromatin binding levels of BETi measured with Click-seq could partly account for BETi responses (AUC 0.63) (fig. S8C), suggesting that differences in drug accessibility contribute to selective BETi effects. Another model attributes transcriptional and therapeutic effects of BETis to their ability to selectively suppress superenhancers (*16*). This notion has been challenged by a recent study that identified H3K27ac-based regulatory potential as a superior predictor of BETi targets (*21*). Because these studies relied on conventional RNA sequencing (RNA-seq) after prolonged drug treatment, we reevaluated both models using SLAM-seq

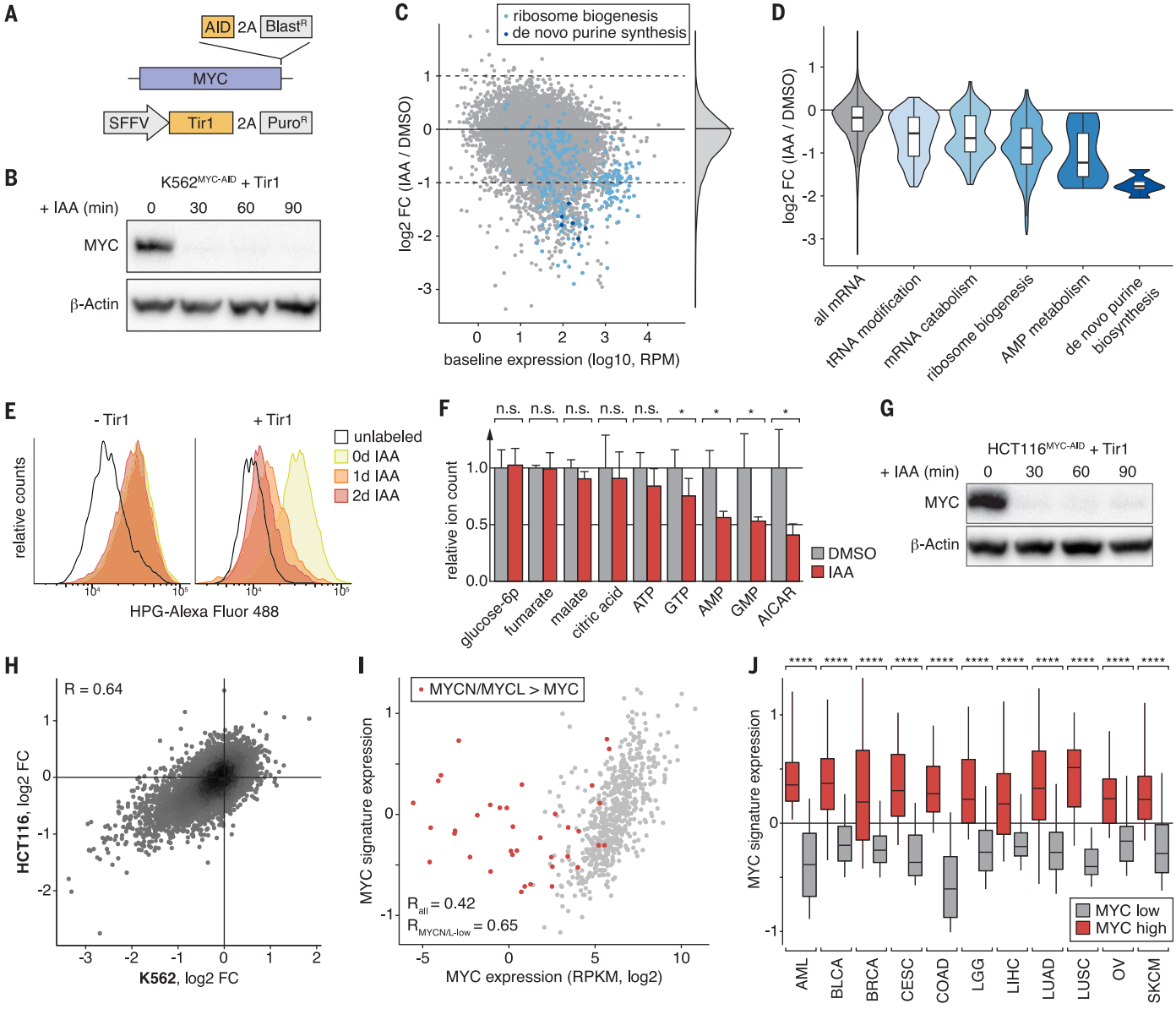

Fig. 3. MYC is a selective transcriptional activator of genes involved in biosynthesis processes. (**A**) Schematic of the MYC-AID knock-in allele and Tir1 delivery vector. (**B**) Immunoblotting of MYC in K562$^{MYC\text{-}AID}$+Tir1 cells treated with IAA. (**C**) SLAM-seq profile after MYC degradation in K562$^{MYC\text{-}AID}$+Tir1 cells (30 min IAA treatment, 60 min 4sU labeling). Highlighted are ribosome biogenesis factors (light blue) and de novo purine synthesis enzymes (dark blue). (**D**) Violin plots depicting SLAM-seq responses of significantly enriched gene ontology classes (Fisher's exact test, FDR-corrected). (**E**) Measurement of global protein synthesis by means of L-homopropargylglycine (HPG) incorporation and flow cytometry in K562$^{MYC\text{-}AID}$ cells treated with IAA. (**F**) Targeted mass spectrometry quantification of indicated metabolites in K562$^{MYC\text{-}AID}$+Tir1 cells after 48 hours of IAA treatment. Bars show means of results from three independent experiments. Error bars indicate 1 SD. n.s., not signficant. *P < 0.05 (Student's t test). (**G**) MYC-immunoblotting in HCT116$^{MYC\text{-}AID}$+Tir1 cells as in (B). (**H**) Comparison of SLAM-seq responses in K562$^{MYC\text{-}AID}$+Tir1 and HCT116$^{MYC\text{-}AID}$+Tir1 cells. (**I**) Expression of *MYC* compared with a signature of the top 100 common MYC-dependent transcripts in (H) across 672 cancer cell lines. (**J**) MYC-target signature expression across 5583 patient samples separated according to high (top 20%) or low (bottom 20%) MYC expression and cancer type. ****P < 0.0001 (Wilcoxon's rank-sum test).

profiles. Both the H3K27ac-based regulatory potential of genes as well as their association with superenhancers (*22*) predicted hypersensitivity to BETis with modest accuracy (AUC 0.66 and 0.64, respectively) (fig. S8B). However, two-thirds of BETi-sensitive genes could not be assigned to superenhancers, and the vast majority of expressed superenhancer-associated genes did not respond to BETi treatment (Fig. 2, F and G). These observations hold true in other leukemia cell lines (fig. S8D) and show that the sensitivity to BET inhibition is associated with, but not determined by, the presence of superenhancers, suggesting that more complex factors underlie this phenomenon.

To further explore determinants of BETi hypersensitivity, we took advantage of extensive profiling data available for K562 cells (*23*, *24*) and devised an unbiased approach for modeling combinatorial modes of gene regulation. Specifically, we extracted signals of 214 ChIP- and methylome-sequencing experiments within 500 and 2000 base pairs (bp) around the TSS of BETi-sensitive and -unresponsive genes and used this data to train various classification models that were later evaluated based on held-out test genes (Fig. 2H and fig. S8E). This approach yielded multiple classifiers that predicted BETi sensitivity with high fidelity (AUC > 0.8) (Fig. 2I and fig. S8F), among them a generalized linear model (GLM) derived through elastic net regression. Reanalyzing coefficients of this model revealed that several factors, including high levels of TSS-proximal REST and H3K27ac, are associated with BETi hypersensitivity, whereas high occupancy of SUPT5H (SPT5), itself a regulator of elongation (*25*, *26*), was the strongest negative predictor (Fig. 2J and fig. S9A). Unsupervised clustering revealed that predictive TFs and cofactors are enriched only at distinct subclusters of BETi-sensitive or -unresponsive genes (Fig. 2J and fig. S9B), suggesting that the transcriptional response to BETis is determined by locus-specific regulators and cannot be predicted on the basis of a single unifying chromatin factor.

Therapeutic effects of BETis are likely mediated through deregulation of multiple hypersensitive genes. Although repression of MYC has been identified as a common and relevant effector mechanism in leukemia (*4*), direct regulatory functions of MYC remain under debate. Previous reports have described activating or repressive effects of MYC on specific target genes, whereas other studies suggest that MYC acts as a general transcriptional amplifier (*27*–*31*). To test these models, we sought to measure direct changes in mRNA output after acute loss of endogenous MYC. We therefore engineered an AID-tag into the endogenous *MYC* locus of K562 cells (Fig. 3A and fig. S10), which in homozygous Tir1-expressing clones allowed for rapid degradation of MYC within less than 30 min (Fig. 3B). We then used SLAM-seq to quantify the output of newly synthesized mRNAs over 60 min after MYC degradation. In contrast to degradation of BRD4, acute loss of MYC resulted in highly specific rather than global changes in mRNA production (Fig. 3C). These were dominated by repressive effects on 712 genes, whereas only 15 mRNAs were strongly up-regulated (fig. S11A). Hence, in K562 cells, MYC does not act as a direct repressor or general amplifier of transcription but predominantly functions as a transcriptional activator of specific target genes.

Because MYC is known to occupy most active promoters (*27*), we next investigated how MYC exerts selective transcriptional activation despite ubiquitous binding. To this end, we trained classification models to predict MYC-dependent transcripts (FDR ≤ 0.1, $\log_2$FC ≤ −1) based on different ChIP-seq signals at their promoter. Elastic net regression yielded a simple GLM that was highly predictive of MYC-dependent gene regulation (AUC 0.91) (fig. S11B). The strongest contributor in this model was the abundance of MYC itself (fig. S11C). Although the presence of MYC at promoters determined by conventional peak calling fails to identify MYC-sensitive transcripts, binding levels of MYC or its cofactor MAX predict MYC-dependent gene regulation with intermediate accuracy (AUC 0.76 and 0.74, respectively) (fig. S11, D and E). These results suggest that genes directly activated by MYC are defined by strong binding of MYC and by further modulation through additional factors such as MNT, NKRF, TBL1XR1, EP300, and YY1.

To investigate the cellular function of MYC-dependent gene regulation, we performed gene ontology analysis of direct MYC target genes in K562 cells. Acute MYC degradation predominantly led to down-regulation of genes associated with protein and nucleotide biosynthesis, including 36% of all ribosome biogenesis factors, key regulators in adenosine 5′-monophosphate (AMP) metabolism, and all six enzymes of the de novo purine synthesis pathway (Fig. 3, C and D, and table S2). MYC degradation progressively impaired protein synthesis (Fig. 3E) and led to a strong reduction in cellular AMP and guanosine 5′-monophosphate (GMP) levels as well as their upstream intermediate aminoimidazole carboxamide ribonucleotide (AICAR) before the onset of cell proliferation defects (Fig. 3F and fig. S12, A and B). MYC's role as a direct regulator of key enzymes in protein and nucleotide biosynthesis—as well as several subunits of RNA polymerases I, II, and III (fig. S12C)—provide an explanation for the reported increase in total cellular RNA upon MYC overexpression and support the notion that these effects are secondary rather than due to global transcriptional effects (*32*).

To test whether direct transcriptional functions of MYC are conserved in other cellular contexts, we introduced homozygous AID-tags into the *MYC* locus of HCT116 human colon carcinoma cells. As with K562 cells, IAA treatment of TIR1-expressing $HCT116^{MYC\text{-}AID}$ cells triggered complete degradation of MYC within less than 30 min (Fig. 3G). SLAM-seq profiling revealed a selective transcriptional response (Fig. 3H and fig. S12D) that affected the same cellular processes (fig. S12E) and correlated with effects observed in K562 cells [Pearson correlation coefficient (R) = 0.64] (Fig. 3H). To test whether the conservation of MYC targets extends to other cancer types, we derived a signature of the 100 most strongly down-regulated genes in SLAM-seq (table S3) and compared its expression with *MYC* levels in a panel of 672 cancer cell lines (*33*). Expression of *MYC* and our MYC target signature correlated well (Fig. 3I), except for a small fraction of outliers. All of these express high levels of *MYCN* or *MYCL* (fig. S13A), indicating that *MYC* paralogs have redundant functions in the regulation of core MYC targets. Our signature of direct MYC targets was also strongly correlated with *MYC* levels in publicly available RNA-seq profiles from 5583 primary patient samples across 11 major human cancers (Fig. 3J and fig. S13B) (*34*). Together, these findings suggest that MYC drives expression of a conserved set of transcriptional targets, which should be considered as entry points for blocking its oncogenic functions.

In summary, combining rapid chemical-genetic perturbation and SLAM-seq establishes a simple yet powerful strategy for probing specific and global direct functions of TFs and cofactors. Using this approach, we functionally characterize BRD4, a protein widely studied as a regulator of lineage- and disease-associated expression programs, as a general cofactor in transcriptional pause-release. We also found that MYC, which has previously been implicated as a global transcriptional amplifier, activates a confined and conserved set of target genes to fuel basic anabolic processes, particularly protein and nucleotide biosynthesis. More generally, by enabling the direct quantification of changes in mRNA output, SLAM-seq provides a simple, robust, and scalable method for defining direct transcriptional responses to any perturbation and thereby exploring the regulatory wiring of a cell.

REFERENCES AND NOTES

1. T. I. Lee, R. A. Young, *Cell* **152**, 1237–1251 (2013).
2. P. A. Jones, J.-P. J. Issa, S. Baylin, *Nat. Rev. Genet.* **17**, 630–641 (2016).
3. J. Shi, C. R. Vakoc, *Mol. Cell* **54**, 728–736 (2014).
4. J. Zuber *et al.*, *Nature* **478**, 524–528 (2011).
5. J. E. Delmore *et al.*, *Cell* **146**, 904–917 (2011).
6. M. A. Dawson *et al.*, *Nature* **478**, 529–533 (2011).
7. C. V. Dang, *Cell* **149**, 22–35 (2012).
8. B. E. Housden *et al.*, *Nat. Rev. Genet.* **18**, 24–40 (2017).
9. B. Schwanhäusser *et al.*, *Nature* **473**, 337–342 (2011).
10. V. A. Herzog *et al.*, *Nat. Methods* **14**, 1198–1204 (2017).
11. P. B. Rahl *et al.*, *Cell* **141**, 432–445 (2010).
12. R. Ren, *Nat. Rev. Cancer* **5**, 172–183 (2005).
13. K. Nishimura, T. Fukagawa, H. Takisawa, T. Kakimoto, M. Kanemaki, *Nat. Methods* **6**, 917–922 (2009).
14. T. Wang *et al.*, *Science* **350**, 1096–1101 (2015).
15. G. E. Winter *et al.*, *Mol. Cell* **67**, 5–18.e19 (2017).
16. J. Lovén *et al.*, *Cell* **153**, 320–334 (2013).
17. P. Filippakopoulos *et al.*, *Nature* **468**, 1067–1073 (2010).
18. P. Rathert *et al.*, *Nature* **525**, 543–547 (2015).
19. C. Y. Fong *et al.*, *Nature* **525**, 538–542 (2015).
20. H. Lu *et al.*, *eLife* **4**, 1–26 (2015).
21. S. Wang *et al.*, *Genome Res.* **26**, 1417–1429 (2016).
22. D. Hnisz *et al.*, *Cell* **155**, 934–947 (2013).
23. ENCODE Project Consortium, *Nature* **489**, 57–74 (2012).
24. S. Mei *et al.*, *Nucleic Acids Res.* **45** (D1), D658–D662 (2017).
25. T. Wada *et al.*, *Genes Dev.* **12**, 343–356 (1998).
26. A. Shetty *et al.*, *Mol. Cell* **66**, 77–88.e5 (2017).
27. C. Y. Lin *et al.*, *Cell* **151**, 56–67 (2012).
28. Z. Nie *et al.*, *Cell* **151**, 68–79 (2012).
29. A. Sabò *et al.*, *Nature* **511**, 488–492 (2014).
30. S. Walz *et al.*, *Nature* **511**, 483–487 (2014).

31. F. Lorenzin *et al.*, *eLife* **5**, 1–35 (2016).
32. T. R. Kress, A. Sabò, B. Amati, *Nat. Rev. Cancer* **15**, 593–607 (2015).
33. C. Klijn *et al.*, *Nat. Biotechnol.* **33**, 306–312 (2015).
34. R. L. Grossman *et al.*, *N. Engl. J. Med.* **375**, 1109–1112 (2016).

ACKNOWLEDGMENTS

We are grateful to all members of the Zuber and Ameres laboratories and A. Stark, F. Muerdter, M. Rath, and D. Kaiser for experimental advice and helpful discussions. We thank A. Sommer, I. Tamir, and the VBCF-NGS team (www.vbcf.ac.at) for deep sequencing services; G. Dürnberger, K. Mechtler, E. Roitinger, and M. Schutzbier at the IMP/IMBA protein biochemistry core facility for performing mass spectrometry–based proteomics; and the IMP/IMBA bio-optics and molecular biology services for continuous support. **Funding:** This work was funded by Starting Grants of the European Research Council to J.Z. (ERC-StG-336860) and S.L.A. (ERC-StG-338252) and the Austrian Science Fund (SFB grants F4710 and F4322, Y-733-B22 START and W127-B09). M.M. is recipient of a DOC fellowship of the Austrian Academy of Sciences. Research at the IMP is generously supported by Boehringer Ingelheim. VBCF is funded by the City of Vienna through the Vienna Business Agency. **Author contributions:** M.M., S.L.A., and J.Z. conceived and planned this project. M.M., A.E., C.U., C.W., T.K., and J.P. designed and conducted experiments. M.M., A.E., T.N., S.L.A., and J.Z. analyzed and interpreted original and publicly available data. T.N. established and performed deep sequencing data analyses. J.J., P.R., V.A.H., B.R., D.A.C., T.H., P.B., and M.F.S. established critical reagents and methodology. J.J.L., A.v.H., A.C.O., and J.P. provided critical input on experimental designs and data analyses. M.M. and J.Z. cowrote the manuscript with input from coauthors. **Competing interests:** S.L.A., B.R., V.A.H., J.Z., and M.M. are inventors on patent application EU17166629.0-1403 submitted by the IMBA that covers methods for the modification and identification of nucleic acids, which have been licensed to Lexogen GmbH. **Data and materials availability:** All deep sequencing data are available through GEO (www.ncbi.nlm.nih.gov/geo) under the accession code GSE111463. Materials will be provided upon request under a materials transfer agreement with IMP.

SUPPLEMENTARY MATERIALS

www.sciencemag.org/content/360/6390/800/suppl/DC1
Materials and Methods
Figs. S1 to S13
Tables S1 to S10
References (*35*–*45*)

5 July 2017; resubmitted 8 February 2018
Accepted 21 March 2018
Published online 5 April 2018
10.1126/science.aao2793

SLAM-seq defines direct gene-regulatory functions of the BRD4-MYC axis

Matthias Muhar, Anja Ebert, Tobias Neumann, Christian Umkehrer, Julian Jude, Corinna Wieshofer, Philipp Rescheneder, Jesse J. Lipp, Veronika A. Herzog, Brian Reichholf, David A. Cisneros, Thomas Hoffmann, Moritz F. Schlapansky, Pooja Bhat, Arndt von Haeseler, Thomas Köcher, Anna C. Obenauf, Johannes Popow, Stefan L. Ameres and Johannes Zuber

Science **360** (6390), 800-805.
DOI: 10.1126/science.aao2793originally published online April 5, 2018

Profiling transcription—a SLAM dunk

Identification of the direct target genes of transcription factors could shed light on how healthy cells become malignant. Muhar *et al.* applied a modified version of a transcript-mapping method called SLAM-seq to identify the target genes of two transcriptional regulators of major interest in cancer research (see the Perspective by Sabò and Amati). The MYC oncoprotein selectively activates transcription of just a few genes, primarily those involved in basic cell metabolism. In contrast, BRD4, a bromodomain-containing protein that is being targeted for cancer therapy, activates transcription of many genes.

Science, this issue p. 800; see also p. 713